Classification of Alzheimer's Disease using Discriminant Manifolds of Hippocampus Shapes

Mahsa Shakeri[1,2], Hervé Lombaert[3], and Samuel Kadoury[1,2]

[1] MEDICAL, Polytechnique Montréal, Montréal, Québec, Canada,
[2] CHU Sainte-Justine Hospital Research Center, Montréal, Québec, Canada,
mahsa.shakeri@polymtl.ca, samuel.kadoury@polymtl.ca,
[3] Inria Sophia-Antipolis Méditerranée, Asclepios Team, Sophia-Antipolis, France,
herve.lombaert@inria.fr

Abstract. Neurodegenerative pathologies, such as Alzheimer's disease, are linked with morphological alterations of subcortical structures which can be assessed from medical imaging and biological data. Recent advances in machine learning have helped to improve classification and prognosis rates. We present here a classification framework for Alzheimer's disease which extracts triangulated surface meshes from segmented binary maps in MRI, and establishes reliable point-to-point correspondences among a population of hippocampus 3D surfaces using their spectral representation. Morphological changes between groups are detected using a manifold learning algorithm based on Grassmannian kernels in order to assess similarity between shape topology in control normals and patients. A second manifold using discriminant embeddings is then generated to maximize the class separability between three clinical groups recognized in dementia. We test the method to classify 47 subjects with Alzheimers Disease (AD), 47 with mild cognitive impairment (MCI) and 47 healthy controls enrolled in a clinical study. Classification rates compare favorably to standard classification methods based on SVM and traditional manifold learning methods evaluated on the same database.

1 Introduction

Alzheimer's disease (AD) is the most common form of dementia, with an incidence that doubles every five years after the age of 65 [2]. As life expectancy increases, the number of AD patients increases accordingly, which causes a heavy socioeconomic burden. It is expected that treatment decisions will greatly benefit from diagnostic and prognostic tools that identify individuals likely to progress to dementia sooner. This is especially important in individuals with mild cognitive impairment (MCI), who present a conversion rate of approximately 15% per year. Towards this end, neuroimaging datasets for AD including magnetic resonance imaging (MRI) and other types of biomarkers have shown considerable promise to detect longitudinal changes in subjects scanned repeatedly over time [13], by offering rich information on the patients morphometric and anatomical profiles. Their use stems from the premise that longitudinal changes may be

more reproducible and more precisely measured with MRI and other parameters such as in clinical scores, cerebrospinal fluid (CSF), or proteomic assessments.

A number of studies reported structural changes in the hippocampus, parahippocampal gyrus, cingulate, and other brain regions in both MCI and AD patients [12]. Other studies have used intensity information to discriminate elderly normal controls (NC) with patients inflicted with AD or mild cognitive impairment (MCI), based on T1-weighted MRI [6]. Previous machine learning algorithms using MRI were based on traditional morphometric measures, such as subcortical volume or shape descriptors of brain structures [3] and their change over time [5]. These were based on finding a low-dimensional representation of complex and high-dimensional data using principal component analysis (PCA) and multidimensional scaling (MDS). However these methods are typically linear, making it easy to transform data from image space into the learned subspace, but lacks the ability to process irregular or abnormal structures, which tend to follow non-linear patterns of variation. To cope with this limitation, manifold learning methods on the other hand tend to better model highly non-linear data, such as from neuroimaging datasets [1]. Recently, discriminant embeddings exploit within and between-class similarities to establish correspondences between disparate data, thereby offering a more accurate relationship of subtile structural alterations in AD.

The objective of this study is to propose a classifier which distinguishes NC subjects from patients with MCI and patients afflicted with AD. First, segmented hippocampus shapes from MRI are matched between each other using a spectral representation of the 3D mesh surface of the sub-cortical surface in order to have one-to-one vertex correspondences between hippocampus shapes throughout a population. Once a training set of hippocampus shapes is created for three clinical relevant groups (NC, MCI, AD), a discriminant manifold based on Grassmannian kernels is trained to maximize the separation between these three groups and improve the classification accuracy for any unseen MRI, which can be processed by mapping the segmented hippocampus onto the trained manifold. Th main contribution of this paper is to develop a hippocamus classification approach based on their spectral representation which is classified in the Grassmannian space.

2 Methods

2.1 Hippocampus shape alignment

In the first step, segmented binary masks obtained from diagnostic T1-weighted MRI are processed to the same image orientation and isotropic voxel sizes, and then converted into 3D triangulated surfaces using the marching cube algorithm. A Gaussian smoothing process is subsequently applied on each surface in order to remove surface irregularities. Then, a reference surface is defined in an iterative process, and all triangulated surfaces are aligned to this reference using a

rigid registration algorithm. In order to establish the point-to-point correspondences across all surfaces, each mesh is matched to a randomly selected reference surface using a spectral matching algorithm as proposed in [8].

The matching between two surfaces S_i and S_j of the hippocampus from two separate subjects is conducted in a two-step process. In the first step, an initial transformation is calculated between the two surfaces, followed by a second step to establish a smooth map between the two meshes based on a diffeomorphic mapping [7]. First, the spectrums of the meshes S_i and S_j are computed according to spectral representation theory. Meshes are described by their principal eigenmodes following an eigendecomposition of their respective Laplacian matrix L. In order to add robustness to the feature matching process, the mean curvature at each point of the mesh defined as $C(i) = 0.5 * (C_{min} + C_{max})$ are calculated, where the principal curvatures C_{min} and C_{max} are estimated as the minimum and maximum curving degrees of a mesh S, respectively. Hence, the mean curvature of C is computed as $\{C(1), C(2), \cdots, C(n)\}$, where n is the number vertices. We incorporate these features in the weighting of the nodes of the spectral graph $\mathcal{G}$ by computing the exponential of the mean curvature, and defining the graph Laplacian as $\tilde{L} = \mathcal{G}L$, where

$$\mathcal{G} = P^{-1}(\exp(diag(\{C(1), C(2), \cdots, C(n)\})))^{-1} \tag{1}$$

and P is the diagonal node degree matrix integrating distance weights. Once meshes are described in the spectral domain, the first e eigenvectors associated with non-zero eigenvalues are chosen to define the spectral representations $\tilde{S}_i$ and $\tilde{S}_j$. After reordering and sign adjustment [7] of the resulting spectrums $\tilde{S}_i$ and $\tilde{S}_j$, we perform non-rigid alignment of the spectral coordinates using Coherent Point Drift (CPD) [9]. The CPD approach finds a continuous transformation between the surfaces $\tilde{S}_i$ and $\tilde{S}_j$ in the spectral domain. Once the two spectral representations are aligned, the point-by-point correspondences between two meshes could be directly established in the Euclidean space, such that the two closest points in the spectral domain are considered as corresponding points in the Euclidean space. Thus, the correspondence map c between S_i and S_j is established with a simple nearest-neighbor search in spectral domain.

It was shown in [8] that incorporating extra features might create discontinuities in the correspondence map c. As a solution, a diffeomorphic matching is applied to find the final map between two shapes. This is obtained by defining an association graph composed of the set of vertices and edges, based on the initial set of correspondence links. The graph Laplacian operator is applied on the resulting graph, followed by a spectral decomposition to produce a shared set of eigenvectors, from which the first and last eigenvalues are used to obtain one-to-one vertex correspondences between the mesh vertices. This procedure is repeated for all training meshes in the three groups of the database, with (1) normal controls, (2) MCI patients and (3) AD patients.

2.2 Learning the discriminant Grassmannian manifold

Manifold learning algorithms are based on the premise that data are often of artificially high dimension and can be embedded in a lower dimensional space. However the presence of outliers and multi-class information can on the other hand affect the discrimination and/or generalization ability of the manifold. We propose to learn the optimal separation between three classes (1) normal controls, (2) MCI patients and (3) AD patients, by using a discriminant graph-embedding based on Grassmannian manifolds for the classification problem initially proposed in [4]. Each sample mesh surface S, which vertices has been rearranged using the alignment method in 2.1, can be viewed as the set of low-dimensional m subspaces of $\mathbb{R}^n$ on a Grassmannian manifold and represented by orthonormal matrices, each with a size of $n \times m$, with n the higher dimensionality of vertices defined earlier. Two points on a Grassmannian manifold are equivalent if one can be mapped into the other one by a $m \times m$ orthogonal matrix. In this work, similarity between two surfaces (S_i, S_j) on the manifold is measured as a combination of projection and canonical correlation Grassmannian kernels $\mathbb{K}_{i,j}$ defined in the Hilbert Space. By describing different features of the hippocampus shape with each kernel, $\mathbb{K}_{i,j}$ can improve discriminatory accuracy between shapes.

In order to effectively discover the low-dimensional embedding, it is necessary to maintain the local structure of the data in the new embedding. The structure $G = (\boldsymbol{V}, \boldsymbol{W})$ is an undirected similarity graph, with a collection of nodes $\boldsymbol{V}$ connected by edges, and the symmetric matrix $\boldsymbol{W}$ with elements describing the relationships between the nodes. The diagonal matrix $\boldsymbol{D}$ and the Laplacian matrix $\boldsymbol{L}$ are defined as $\boldsymbol{L} = \boldsymbol{D} - \boldsymbol{W}$, with $\boldsymbol{D}(i,i) = \sum_{j \neq i} \boldsymbol{W}_{ij} \forall i$. Here, N labelled points $\mathbb{S} = \{(S_i, c_i)\}_{i=1}^{N}$ are generated from the underlying manifold $\mathcal{M}$, where c_i denotes the label (NC, MCI or AD). The task at hand is to maximize a measure of discriminatory power by mapping the underlying data into a vector space, while preserving similarities between data points in the high-dimensional space. Discriminant graph-embedding based on locally linear embedding (LLE) [11] uses graph-preserving criterions to maintain these similarities, which are included in a sparse and symmetric $N \times N$ matrix, denoted as M.

Within and between similarity graphs: In our work, the geometrical structure of $\mathcal{M}$ can be modeled by building a within-class similarity graph $\boldsymbol{W}_w$ for hippocampus of same group and a between-class similarity graph $\boldsymbol{W}_b$, to separate hippocampus from the three classes. When constructing the discriminant LLE graph, elements are partitioned into $\boldsymbol{W}_w$ and $\boldsymbol{W}_b$ classes. The intrinsic graph G is first created by assigning edges only to samples of the same class (ex: MCI). The local reconstruction coefficient matrix $M(i,j)$ is obtained by minimizing:

$$\min_{M} \sum_{j \in \mathcal{N}_w(i)} \|S_i - M(i,j) S_j\|^2 \quad \sum_{j \in \mathcal{N}_w(i)} M(i,j) = 1 \;\; \forall i \tag{2}$$

with $\mathcal{N}_w(i)$ as the neighborhood of size k_1, within the same region as point i (e.g. hippocampus from MCI patient). Each sample is therefore reconstructed only from 3D meshes of the same clinical group. The local reconstruction coefficients are incorporated in the within-class similarity graph, such that the matrix $\boldsymbol{W}_w$ is defined as:

$$W_w(i,j) = \begin{cases} (M + M^T - M^T M)_{ij}, & \text{if } \ S_i \in \mathcal{N}_w(S_j) \text{ or } x_j \in \mathcal{N}_w(S_i) \\ 0, & \text{otherwise.} \end{cases} \tag{3}$$

Conversely, the between-class similarity matrix $\boldsymbol{W}_b$ depicts the statistical properties to be avoided in the optimization process and used as a high-order constraint. Distances between healthy and pathological samples are computed as:

$$W_b(i,j) = \begin{cases} 1/k_2, & \text{if } S_i \in \mathcal{N}_b(S_j) \text{ or } S_j \in \mathcal{N}_b(S_i) \\ 0, & \text{otherwise} \end{cases} \tag{4}$$

with $\mathcal{N}_b$ containing k_2 neighbors having different class labels from the ith sample. The objective is to transform points to a new manifold $\mathcal{M}$ of dimensionality d, i.e. $S_i \rightarrow y_i$, by mapping connected samples from the same group in $\boldsymbol{W}_w$ as close as possible to the class cluster, while moving NC, MCI and AD meshes of $\boldsymbol{W}_b$ as far away from one another. This results in optimizing the objective functions:

$$f_1 = \min \frac{1}{2} \sum_{i,j} (y_i - y_j)^2 W_w(i,j) \qquad f_2 = \max \frac{1}{2} \sum_{i,j} (y_i - y_j)^2 W_b(i,j) \tag{5}$$

Supervised manifold learning: The optimal projection matrix, mapping new points to the manifold, is obtained by simultaneously maximizing class separability and preserving interclass manifold property, as described by the objective functions in Eq.(5). Assuming points on the manifold are known as similarity measures given by the Grassmannian kernel $\mathbb{K}_{i,j}$, a linear solution can be defined, i.e., $y_i = (\langle \alpha_1, S_i \rangle, \ldots, \langle \alpha_r, S_i \rangle)^T$ for the r largest eigenvectors with $\alpha_i = \sum_{j=1}^{N} a_{ij} S_j$. Defining the coefficient $\boldsymbol{A}_l = (a_{l1}, \ldots, a_{lN})^T$ and kernel $\boldsymbol{K}_i = (k_{i1}, \ldots, k_{iN})^T$ vectors, the output can be described as $y_i = \langle \alpha_l, S_i \rangle = \boldsymbol{A}_l^T \boldsymbol{K}_i$. By replacing the linear solution in the minimization and maximization of the between- and within-class graphs, the optimal projection matrix $\mathbb{A}$ is acquired from the optimization of the function as proposed in [4]. The proposed algorithm uses the points on the Grassmannian manifold implicitly (i.e., via measuring similarities through a kernel) to obtain a mapping $\mathbb{A}$. The matrix maximizes a quotient similar to discriminant analysis, while retaining the overall geometrical structure. Hence for any new segmented surface mesh S_q, a manifold representation can be obtained using the kernel function based on S_q and mapping $\mathbb{A}$.

3 Experiments and results

We used the Alzheimer's Disease Neuroimaging Initiative (ADNI) database with 1.5 or 3.0 T structural MR images (adni.loni.usc.edu). For this study, a subset of baseline 1.5 T MR images is used including 47 normal controls (NC), 47 AD patients, and 47 individuals with MCI. The three groups are matched approximately by age and gender (NC with a mean age of 76.7 ± 5.4, 23 male; AD with a mean age of 77.4 ± 7.2, 21 males; MCI with a mean age of 75.0 ± 6.9, 28 males). Additional post-processing steps were performed on the MR images to correct certain image artifacts and to enhance standardization across sites and platforms. The post-processing steps include gradient non-linearity correction, intensity inhomogeneity correction, bias field correction, and phantom-based geometrical scaling to remove calibration errors. Here, we use these processed images. Left and right hippocampi were segmented using FSL-FIRST automatic segmentation [10] and visual inspection was performed on the output binary masks to ensure the quality of the segmentation. Fig. 1 shows the shape differences in the left and right hippocampus between NC, MCI and AD.

The optimal size was found at $k_1 = 7$ for within-class neighborhoods ($\mathcal{N}_w$), and $k_2 = 4$ for between-class neighborhoods ($\mathcal{N}_b$). The optimal manifold dimensionality was set at $d = 5$, when the trend of the nonlinear residual reconstruction error curve stabilized for the entire training set. Fig. 2 shows the resulting manifold with embedded hippocampus shapes which can be clearly identified into three separate groups, due to the discriminative nature of the framework. Table 1 presents accuracy, sensitivity and specificity results for SVM (nonlinear RBF kernel), LLE and the proposed method between three clinically relevant pairs of diagnostic groups (NC/AD, NC/MCI, MCI/AD). The classifier performance was obtained by repeating 100 times a random selection of samples, using 75% of the data for training and 25% for testing in each run. Results show a significant improvement using the discriminant manifold embedding compared to standard approaches. It also illustrates that increased accuracy can be achieved using the discriminant embedding with combined kernel ($\alpha_1 = 1, \alpha_2 = 5$), which suggests the benefit of extracting complementary features from the dataset for classification purposes compared to different types of classification models (SVM, LLE).

4 Conclusion

Our main contribution consists in describing morphometric variations of the hippocampus in a discriminant nonlinear graph embedding with Grassmannian manifolds to detect the presence of Alzheimer's disease. A spectral matching process based on the eigendecomposition of the Laplacian matrix of hippocampus shapes extracted from a dataset of MRI images enabled to establish one-to-one correspondences in mesh vertices. This is critical to construct a reliable training set of sub-cortical shapes from various pathological groups and normal controls. A manifold embedding including intrinsic and penalty graphs measuring

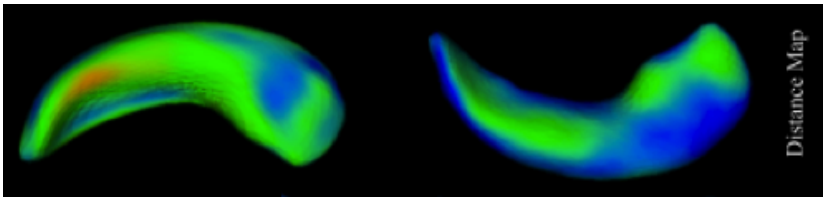

(a)

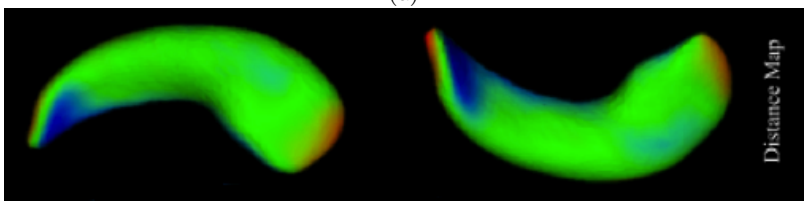

(b)

Fig. 1: (a) Distance maps of left and right hippocampal shape deformations in AD patients compared with normal controls. (b) Distance maps of left and right hippocampal shape deformations in MCI patients compared with normal controls.

Table 1: Classification results for the classification of NC, MCI and AD patients from segmented hippocampal regions. We compare a standard SVM classification approach, with a single LLE method and the proposed discriminant LLE method.

	NC/AD			NC/MCI			MCI/AD			All groups		
	SVM	LLE	**DLLE**	SVM	LLE	**DLLE**	SVM	LLE	**DLLE**	SVM	LLE	**DLLE**
Sensitivity tp/(tp+fn)	0.75	0.84	**0.90**	0.58	0.61	**0.69**	0.50	0.57	**0.60**	0.61	0.67	**0.73**
Specificity tn/(tn+fp)	0.69	0.77	**0.85**	0.62	0.70	**0.77**	0.57	0.61	**0.67**	0.62	0.69	**0.77**
Overall accuracy	0.72	0.79	**0.88**	0.60	0.65	**0.72**	0.54	0.58	**0.65**	0.62	0.67	**0.74**

similarity within clinical relevant groups and between NC, MCI and AD patients, respectively, was trained to differentiate between the different hippocampus shapes. A combination of canonical correlation kernels creates a secondary manifold to simplify the deviation estimation from normality, improving detection of pathology compared to standard LLE. Experiments show the need of nonlinear embedding of the learning data, and the relevance of the proposed method for stratifying different stages of dementia progression. In the context of Alzheimer's disease, the method can improve for the early detection of the disease with promising classification rates based on ground-truth knowledge. Future work will compare results to volumetric measurements and improve the deviation metric using high-order tensorization and investigate into fully automated hippocampus segmentation, as it can affect the precision of the spectral correspondence process.

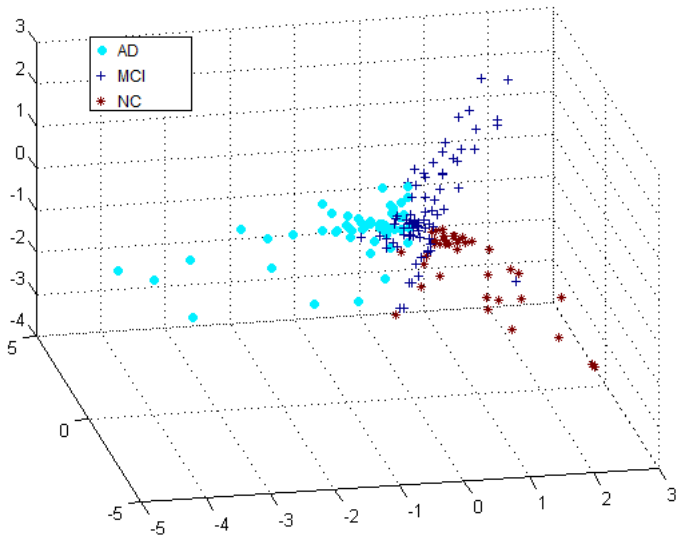

Fig. 2: Resulting manifold embedding with low-dimensional coordinates of samples points taken from the NC, MCI and AD groups.

References

1. Aljabar, P., Wolz, R., Srinivasan, L., Counsell, S.J., Rutherford, M.A., Edwards, A.D., Hajnal, J.V., Rueckert, D.: A combined manifold learning analysis of shape and appearance to characterize neonatal brain development. IEEE Transactions on Medical Imaging 30(12), 2072–2086 (2011)
2. Bain, L., Jedrziewski, K., Morrison-Bogorad, M., et al.: Healthy brain aging: A meeting report from the Sylvan M. Cohen Annual Retreat of the University of Pennsylvania Institute on Aging. Alzheimers Dementia 4, 443–446 (2008)
3. Chupin, M., Hammers, A., Liu, R.S., Colliot, O., Burdett, J., Bardinet, E., Duncan, J.S., Garnero, L., Lemieux, L.: Automatic segmentation of the hippocampus and the amygdala driven by hybrid constraints: method and validation. Neuroimage 46(3), 749–761 (2009)
4. Harandi, M., Sanderson, C., et al.: Graph embedding discriminant analysis on grassmannian manifolds for improved image set matching. In: CVPR. p. 2705 (2011)
5. Leow, A.D., Yanovsky, I., Chiang, M.C., Lee, A.D., Klunder, A.D., Lu, A., Becker, J.T., Davis, S.W., Toga, A.W., Thompson, P.M.: Statistical properties of jacobian maps and the realization of unbiased large-deformation nonlinear image registration. IEEE Transactions on Medical Imaging 26(6), 822–832 (2007)
6. Li, Y., Wang, Y., Wu, G., Shi, F., Zhou, L., Lin, W., Shen, D., Initiative, A.D.N., et al.: Discriminant analysis of longitudinal cortical thickness changes in alzheimer's disease using dynamic and network features. Neurobiology of aging 33(2), 427–e15 (2012)

7. Lombaert, H., Grady, L., Polimeni, J.R., Cheriet, F.: FOCUSR: feature oriented correspondence using spectral regularization–a method for precise surface matching. IEEE Trans. Pattern Anal. Mach. Intell. 35, 2143–60 (9 2013)
8. Lombaert, H., Sporring, J., Siddiqi, K.: Diffeomorphic Spectral Matching of Cortical Surfaces. In: Information Processing in Medical Imaging. pp. 376–389 (2013)
9. Myronenko, A., Song, X., Miguel, A.C.: Non-rigid point set registration:Coherent Point Drift. IEEE Trans. Pattern Anal. Mach. Intell. 32, 2262–2275 (12 2009)
10. Patenaude, B., Smith, S.M., Kennedy, D.N., Jenkinson, M.: A bayesian model of shape and appearance for subcortical brain segmentation. Neuroimage 56(3), 907–922 (2011)
11. Roweis, S., Saul, L.: Nonlinear dimensionality reduction by locally linear embedding. Science 290, 2323–6 (2000)
12. Visser, P., Verhey, F., Hofman, P., Scheltens, P., Jolles, J.: Medial temporal lobe atrophy predicts alzheimer's disease in patients with minor cognitive impairment. Journal of Neurology, Neurosurgery & Psychiatry 72(4), 491–497 (2002)
13. Wyman, B.T., Harvey, D.J., Crawford, K., Bernstein, M.A., Carmichael, O., Cole, P.E., Crane, P.K., DeCarli, C., Fox, N.C., Gunter, J.L., et al.: Standardization of analysis sets for reporting results from adni mri data. Alzheimer's Dementia 9(3), 332–337 (2013)